Redox Biology 86 (2025) 103804

Contents lists available at ScienceDirect

Redox Biology

journal homepage: www.elsevier.com/locate/redox

Nrf2/Nlrp3 signaling in aging BMSCs: Traf6 intervention as a novel approach to osteoporosis treatment

Yajun Li [a,1], Yunshang Yang [a,1], Donglong Xia [a,1], Yiling Fang [b], Cheng Tang [a], Jingxian Yu [a], Dechun Geng [c,*], Zhirong Wang [a,**], Long Xiao [a,***]

[a] Translational Medicine Innovation Center, Zhangjiagang TCM Hospital Affiliated to Nanjing University of Chinese Medicine, Zhangjiagang, 215600, China
[b] Department of General Practice, The First People's Hospital of Zhangjiagang, Soochow University, Zhangjiagang, 215600, China
[c] Department of Orthopedics, The First Affiliated Hospital of Soochow University, Suzhou, 215006, China

ARTICLE INFO

Keywords:
Senile osteoporosis
Inflammatory senescence
Traf6
Nlrp3 inflammasome
Oxidative stress

ABSTRACT

Senile osteoporosis progression is closely related to the decreased osteogenic differentiation capacity of senescent bone marrow stromal stem cells (BMSCs). This study demonstrated that the Traf6-mediated Nrf2/Nlrp3 signaling axis significantly influences inflammatory senescence progression in BMSCs, and targeting Traf6 can effectively alleviate bone loss caused by inflammatory senescence. High-throughput sequencing revealed that primary BMSCs from 18Ms mice were differentially enriched in anti-inflammatory, antioxidant, and immune-related biological processes compared to those from young mice, with significant differences in the protein expression of Traf6, Nrf2, and Nlrp3-related pathways, indicating potential crosstalk. In vitro experiments using western blotting and immunofluorescence confirmed high levels of intracellular inflammation, oxidative stress, and elevated expression of Traf6, Nrf2, and Nlrp3 inflammatory vesicles in senescent BMSCs. We used lentiviral transfection to knockdown Traf6 and intervention with Nrf2 agonists and inhibitors, and we verified the regulation of the expression of Nrf2/Nlrp3 inflammatory vesicles by Traf6 and its effect on inflammatory senescence progression in BMSCs. We performed in vivo experiments involving targeted Traf6 knockdown in bone tissue, morphological analysis of the femur by micro-computed tomography and immunohistochemistry, measurement of serum MDA and bone metabolism-related indices using ELISA, and calcein labeling to observe the calcium salt deposition rate. These experiments confirmed that the Traf6-mediated Nrf2/Nlrp3 signaling axis significantly influences the inflammatory senescence of BMSCs. Targeting Traf6 effectively alleviates bone loss caused by inflammatory senescence, presenting a potential method for preventing and controlling senile osteoporosis.

1. Introduction

As society ages, the prevalence and disability rate of senile osteoporosis (SOP) increases annually; therefore, it is crucial to prevent and mitigate its onset and progression to reduce its social burden. The progression of SOP is associated with a variety of factors within the bone microenvironment, including inflammation, elevated levels of oxidative stress leading to enhanced osteoclast activity, and reduced osteogenic capacity of senescent BMSCs. Studies have shown that senescence is closely related to inflammation, with high levels of aseptic inflammation in senescent cells disrupting the intracellular environment and accelerating inflammatory senescence [1]. High-throughput sequencing revealed that primary BMSCs from 18-month-old mice were enriched in genes related to anti-inflammatory, antioxidant, and immune-related biological processes and NF-κB and MAPK pathways compared to those from young mice. Additionally, the transcript levels of pro-inflammatory factors, such as TNF-α, IL-1β, IL-6, and NOD-like receptor protein 3 (Nlrp3), were significantly upregulated.

Nlrp3 inflammatory vesicles, as intrinsic intracellular immune receptors, play a key role in the inflammatory response. Their associated components, including Nlrp3, pro-IL-1β, and pro-IL-18, are regulated by upstream proteins mediated by transcription factors, such as TLRs,

* Corresponding author.
** Corresponding author.
*** Corresponding author.
E-mail addresses: szgengdc@suda.edu.cn (D. Geng), zjgfy_spine_wzr@njucm.edu.cn (Z. Wang), zjgfy_spine_xl@njucm.edu.cn (L. Xiao).
[1] First authors with equal contribution.

https://doi.org/10.1016/j.redox.2025.103804
Received 11 June 2025; Received in revised form 23 July 2025; Accepted 30 July 2025
Available online 31 July 2025

Traf6, and NF-κB [2]. Traf6 is a key junction protein in the intracellular signaling pathway, and when pattern recognition receptors, TLRs, are activated by extracellular signals, Traf6 is recruited; this initiates an intracellular signaling cascade that triggers the NF-κB pathway and promotes the assembly of Nlrp3 inflammatory vesicles [3]. Cellular injury-related events, such as reactive oxygen species (ROS) accumulation and mitochondrial dysfunction, activate Nlrp3 inflammatory vesicles, releasing IL-1β and IL-18, which mediate the upregulation of these cytokines [4]. These fluctuations in inflammation and oxidative stress levels are closely related to the Nrf2 pathway, a central transcription factor that regulates the expression of several cytoprotective genes in cells and plays a key role in anti-inflammatory and antioxidant activities. Previous studies have confirmed the presence of increased Traf6 expression levels and significantly decreased Nrf2 expression levels in senescent cells [5,6]. Additionally, complex crosstalk exists between Traf6-mediated NF-κB and MAPK pathways and Nrf2 transcriptional regulation [7,8]. The modulation of Nrf2/Nlrp3 expression by Traf6 in senescent BMSCs and its impact on inflammatory senescence progression remain unclear.

Therefore, this study aimed to establish an in vitro model of inflammatory senescent BMSCs and verify the pro-inflammatory/anti-inflammatory imbalance within their intracellular microenvironment. We further confirmed abnormal upregulation in inflammatory factors, such as Traf6, Nlrp3, IL-1β, and IL-18, alongside a significant decrease in Nrf2 expression levels. In vitro, interference with LV-shtraf6 suppressed Nlrp3 expression, inflammation levels, and senescence progression in BMSCs while significantly enhancing osteogenic function compared to controls. These effects were significantly reversed after the intervention with the Nrf2 inhibitor. In vivo, the inflammatory senescence mouse model treated with an intramedullary LV-shtraf6 injection exhibited accelerated osteogenesis and increased bone volume compared to controls, and Nlrp3 expression and inflammation levels in bone tissue were significantly reduced. The findings indicate that the Traf6-mediated Nrf2/Nlrp3 signaling axis influences inflammatory senescence progression in BMSCs, and Traf6-targeted intervention can effectively alleviate bone loss caused by inflammatory senescence, suggesting a potentially effective treatment for SOP.

2. Materials and methods

2.1. Isolation and extraction of mouse BMSCs

Mice were killed, soaked in 75 % medical alcohol for 5–10 min, and transferred to an ultra-clean bench. The bilateral femur and tibia were aseptically separated, and the bone tissue was transferred to a Petri dish containing phosphate buffer saline (PBS). The bone ends were cut off, and the bone marrow was rinsed in a culture medium using a syringe. The bone marrow suspension was filtered through a 200-mesh sieve, made into a single-cell suspension with a complete culture medium, and then incubated for 48 h. The unattached cells were discarded. Subsequently, the fluid was changed once every 2–3 d, and cell growth and integration were observed. Passaging was initiated once cell integration reached 80 %. All cells were initially cultured in Dulbecco's Modified Eagle Medium (DMEM) containing 10 % fetal bovine serum (16140071, Gibco, Rockville, USA) and 100 U/mL penicillin-streptomycin-amphotericin B (C100C8, NCM Biotech, Suzhou, China) before plate seeding and drug intervention. Subsequently, they were incubated in DMEM (SH30022.01, Cytiva, Pittsburgh, USA) for passaging, with the medium changed every other day.

2.2. Cell viability assay

BMSCs at passage 3 activity was determined using the CCK-8 viability assay. BMSCs were seeded at a density of 1×10^4 in 96-well plates (3599, Corning, ME, USA) and incubated (at 37 °C and 5 % CO2) for 1, 2, 3, 5, or 7 days. Thereafter, 10 μL of CCK-8 buffer (CK04, DOJINDO Laboratories, Tokyo, Japan) was added to each well and incubated at 37 °C thermostat for 1 h. After incubation, absorbance was measured at 450 nm using enzyme-linked immunosorbent assay (ELISA) (ELX800, BioTek, Vermont, USA). The cytotoxicity assay was performed 24 h after BMSCs were seeded at 1×10^5 density in 96-well plates and treated with different concentrations of TBHQ (HY-100489, MCE, Shanghai, China) and ML385 (HY-100523, MCE, Shanghai, China) for 1 or 2 days, respectively, followed by 10 μL per well of CCK-8 buffer for 1 h; subsequently, the absorbance was measured.

2.3. Western blot (WB)

BMSCs at passage 3 were seeded into 6-well plates (3516, Corning, ME, USA) at a density of 1×10^5 cells/well. After grouping and intervention, Ripa lysis buffer containing protease inhibitors and phosphatase inhibitors was used to extract proteins, and BCA method was used to determine the protein concentration. Then the prepared protein solution was mixed with 5x loading buffer and boiled for 10 min. Protein samples were separated in an electrophoresis apparatus and transferred onto a PVDF membrane (IPVH00010, Millipore Corporation, Billerica, USA). The membrane was sealed with a sealing solution for 15 min and incubated with primary antibodies at 4 °C overnight. The following antibodies were used (see Table 1): traf6 (1:1000, ab33915, Abcam, Cambridge, UK), Nrf2 (1:1000, 12721s, CST, Boston, USA), senescence-associated proteins p16 (1:1000, ab211542, Abcam, Cambridge, UK), p21 (1:1000, ab109199)and p53 (1: 1000, ab26), osteogenic functional proteins Runx2 (1:1000, ab192256, Abcam) and Osx (1:1000, ab209484, Abcam), inflammatory vesicle-associated proteins Nlrp3 (1:1000, ab263899, Abcam), IL-1β (1:1000, ab254360, Abcam), and IL-18 (1:1000, ab207323, Abcam). After washing with TBST (BP-G0004, CWBiotech, Beijing, China), the membranes were incubated with secondary antibodies for 2 h. Finally, the membranes were developed with chemiluminescent HRP substrate (WBKLS0500, Millipore Corporation, Massachusetts, USA).

2.4. ALP, ARS, and oil red O staining

BMSCs at passage 3 were seeded into 12-well plates (3513, Corning, ME, USA). After cell proliferation, they were cultured in an osteogenic induction medium (Cyagen Biosciences, Guangzhou, China) for 7 days, with the culture medium being changed every 3 days. Following this, cells were washed with PBS and fixed in 4 % paraformaldehyde solution for 30 min at room temperature. ALP staining working solution was added and incubated at 37 °C for 30 min. The cells were then washed twice with ddH_2O, and observed and photographed under a microscope. After 14–21 days of osteogenic/lipogenic induction, cells were gently washed twice or thrice with PBS. Then, ALP/ARS or oil red staining working solution in 4 % paraformaldehyde was added to each well and allowed to stain for 10 min at room temperature. Afterward, incubation at 37 °C for 30 min ensued, followed by observation and photography after washing. In the statistical analysis stage, we used ImageJ software to analyze ALP, ARS, and oil red data. Three visual fields were randomly selected from each group, and the proportion of staining positive area in the total visual field area was analyzed with software [9].

2.5. Flow cytometry

Cells from each group were seeded in 12-well plates at 5×10^5/mL/well. After 3 days of group intervention, the medium was removed and replaced with 500 μL of fresh medium containing 1.5 μL of senescence dye (ab228562, Abcam) and incubated for 1–2 h at 37 °C in a constant temperature oven protected from light. After the incubation period, cells were washed twice with Assay Buffer XXVII/Wash Buffer, trypsinized, washed once with Assay Buffer XXVII/Wash Buffer, and analyzed via flow cytometry using an excitation wavelength of 488 nm. Fluorescence intensity was detected using the FITC fluorescence channel (green).

Table 1
Antibody information.

Antibodies	Source	Identifier	Ratio
Anti-Traf6 rabbit monoclonal	Abcam	Cat#ab33915; RRID: AB_778572	WB:1:1000 IF:1:100
Anti-CDKN2A/p16INK4a Rabbit monoclonal	Abcam	Cat #ab211542 RRID: AB_2891084	WB:1:1000
Anti-P53 mouse monoclonal	Abcam	Cat#ab26 RRID: AB_303198	WB:1:1000 IF:1:100
Anti-Runx2 rabbit monoclonal	Abcam	Cat #ab192256 RRID: AB_2713945	WB:1:1000
Anti-Osterix rabbit monoclonal	Abcam	Cat#ab209484 RRID: AB_2892207	WB:1:1000 IF:1:100
Anti-Nlrp3 rabbit monoclonal	Abcam	Cat# ab263899 RRID: AB_2889890	WB:1:1000
Anti-IL-1 β rabbit monoclonal	Abcam	Cat# ab254360 RRID: AB_2936299	WB:1:1000
Anti-IL-18 rabbit monoclonal	Abcam	Cat# ab207323 RRID: AB_2895063	WB:1:1000
Anti-P21 mouse monoclonal	Abcam	Cat#ab109199 RRID: AB_10861551	WB:1:1000
Anti-Nrf2 rabbit monoclonal	Cell Signaling Technology	Cat#12721 RRID: AB_2715528	WB:1:1000 IF:1:100
Anti-Nlrp3 rabbit monoclonal	Thermo Fisher Scientific	Cat#MA5-32255 RRID: AB_2809541	IF:1:100
Anti-P65 rabbit monoclonal	Abcam	Cat#ab32536 RRID: AB_776751	WB:1:1000
Anti-pP65 rabbit monoclonal	Abcam	Cat#ab76302 RRID: AB_1524028	WB:1:1000
Anti-ERK rabbit monoclonal	Abcam	Cat#ab184699 RRID: AB_2802136	WB:1:1000
Anti-pERK rabbit monoclonal	Abcam	Cat#ab201015 RRID: AB_2934088	WB:1:1000
Anti-JNK rabbit monoclonal	Abcam	Cat#ab179461 RRID: AB_2744672	WB:1:1000
Anti-pJNK rabbit monoclonal	Abcam	Cat#ab4821 RRID: AB_2141012	WB:1:1000
Anti-P38 rabbit monoclonal	Abcam	Cat#ab170099 RRID: AB_3083680	WB:1:1000
Anti-pP38 rabbit monoclonal	Abcam	Cat#ab195049 RRID: AB_2576214	WB:1:1000

2.6. Lentiviral transfection

This experiment was outsourced to Genepharma (Shanghai, China) to construct lentiviral particles (5′ to 3′ sequences in Table 2). BMSCs at passage 3 were trypsinized with 0.25 % trypsin-EDTA, centrifuged, and the cells were seeded into 6-well plates containing medium without antibiotics at a density of 1×10^5 per well. When the confluence of cells was 60 %, the medium was replaced with 2 mL of fresh medium containing 6 μg/mL polybrene. Subsequently, the lentiviruses, with a value of 50, were added at the designated MOI for transfection, which proceeded for 24 h. After 24 h, the medium was completely replaced with a virus-free complete medium, and knockdown efficiency was verified via WB experiments by observing under an inverted microscope on alternate days. In subsequent experiments, we established a senescence + lentiviral null group (LV-nc) group and performed functional recovery experiments to effectively rule out abnormal expression levels of relevant pathway and functional proteins caused by non-specific gene editing.

Table 2
Lentivirus sequences.

Lentivirus 5 to 3 sequence	
LV-nc	TTCTCCGAACGTGTCACGT
LV-603	GCAAGTATGAGTGTCCCATCT
LV-773	GCAAAGCGAGAGATTCTTTCC
LV-900	GCCAACGTCCTTTCCAGAAGT

2.7. Immunofluorescence staining

Groups of BMSCs at passage 3 were seeded in 12-well plates, and differentiated osteoblasts were washed three times in succession with PBS, fixed with 4 % paraformaldehyde for 30 min, and permeabilized with Triton X-100 for 10 min. They were then incubated with anti-Nrf2 primary antibody at 4 °C overnight, followed by Alexa Fluor 555 secondary antibody (1:1000, ab150078, abcam) for 1 h in the dark. After fixation with a DAPI-containing blocking solution for 10 min, fluorescence intensity was quantitatively analyzed by imaging using an EVOS M5000 cell imaging system (Thermo Fisher Scientific, Bothell, WA, USA).

2.8. Animal models and pharmacological interventions

The current view is that minimizing the likelihood of both Type I and Type II errors requires the largest possible sample size, and that exceeding the required sample size leads to a waste of resources and the ethical issue of sacrificing animals. In the present study, we used a resource equation approach to determine a sample size of 5 for each dataset [10]. The data of each group were measured and averaged by three researchers to reduce subjective errors; additionally, we ensured three replicates of each group in the in vitro experiments, which is consistent with the design of animal experiments and sample size used for in vitro experiments in the current mainstream journals [11–13]. All animal experiments in this study were approved by the Institute of Animal Care Committee of Zhangjiagang City Hospital of Traditional Chinese Medicine (approval number: 20210913). Forty-six experimental C57BL/6J mice were purchased from the JOINN Laboratory, Suzhou, China, with an average weight of approximately 20 g. We randomly divided the mice into four groups of 10 mice each. Five of them were used for calcein labeling to analyze calcium salt deposition rates, and the other five were used for immunohistochemical staining analyses due to the presence of fluorescence interference from calcein labeling. The remaining six mice were used to verify the efficiency of lentiviral transfection. The following groups were formed: 6-week-old group (control group), senescence model group (D-Gal group), senescence + lentiviral null group (LV-nc group), and senescence + Traf6 knockdown(LV-shtraf6 group). After pentobarbital anesthesia, mice in the LV-nc and LV-shtraf6 groups underwent bilateral anterior knee skin incision. A longitudinal incision was made along the medial side of the patellar ligament, displacing the patella laterally to expose the femoral intercondylar space. The proximal part of the femoral condyles was punctured with a 0.25 mm diameter syringe needle along the long axis using the Hamilton microinjector (80401, Hamilton Bonadoutz, Switzerland). A feeding needle (33G, Hamilton) was used to inject an equal volume of virus fluid into the marrow cavity, and the opening was closed with bone wax and sutured layer by layer. We selected the lentiviral-transfected group of mice, harvested the cells 1 week after modeling, and verified the knockdown efficiency under fluorescence microscopy after wall attachment. After the transfection knockdown efficiency was determined to be satisfactory, mice in the D-Gal and LV-shtraf6 groups were injected subcutaneously with D-Galactose

(HY–N0210, MCE, Shanghai, China) at 150 mg/kg/d [14]. Five mice in each group were injected intraperitoneally with 10 mg/kg calcein (HY-D0040, MCE, Shanghai, China) 10 and 3 days before harvesting, and the undecalcified hard tissue sections were taken in time after taking the materials. The calcium salt deposition line formed on the bone surface after the above two intraperitoneal injections was observed under a fluorescence microscope. The field of view was randomly selected and the distance between two parallel deposition lines was measured to analyze the average daily calcium salt deposition thickness. Calcium salt deposition rate = (the distance between two calcium salt deposition lines)/7d. After 8 weeks of pharmacological intervention in mice, we collected blood from their orbits, centrifuged the top serum layer, and performed ELISA experiments to analyze the expression levels of bone turnover markers, OCN and CTX-1, and inflammation-related factor, IL-1β. Five unlabeled calcein femurs from the remaining groups were fixed in 4 % paraformaldehyde for 48 h and assessed using micro-computed tomography (CT), followed by histological and immunofluorescence analysis.

2.9. ELISA

Peripheral blood serum markers of bone metabolism and inflammation were assessed using ELISA kits according to manufacturer instructions. Peripheral blood serum supernatant levels of OCN, CTX-1, and inflammatory factors were determined using standards (100 μL) and test (100 μL) samples added to designated wells and incubated at 37 °C for 15 min. After discarding the contents, wells were washed three times, followed by the addition of a biotinylated antibody working solution (100 μL/well). Plates were then incubated at 37 °C for 30 min, after which the liquid was discarded, and the plates were washed again. Biotinylated antibody working solution (100 μL) was added to each well, incubated at 37 °C for 60 min, and the plate was washed three times. HRP enzyme conjugate working solution (100 μL) was added to each well and incubated at 37 °C for 30 min. The liquid in the plate was discarded, and the plate was washed five times. Substrate solution (90 μL) was added to each well and incubated at 37 °C for 15 min; the termination solution (50 μL) was added to each well. After zeroing with a blank well, the absorbance (OD value) was measured at 450 nm using ELISA, and the sample concentration was calculated.

2.10. Micro-CT

The right femur and lumbar vertebrae of each mouse was scanned and analyzed using a SkyScan1176 high-resolution micro-CT scanner (SkyScan, Knotich, Belgium). Scanning parameters were set to 9 μm per slice, voltage to 80 kV, and current to 100 mA. After the scanning, the bone trabeculae within 2 mm below the growth plate in the epiphysis of the femoral shaft was selected in CTAn software (brukermicro CT, kontich, Belgium) as the area of interest (ROI) for three-dimensional reconstruction. Measure and analyze distal femoral bone mineral density (BMD, g/cm^3), bone surface,(BS, mm^2), bone volume/total volume (BV/TV, %), trabecular bone thickness (Tb. Th, 1/mm), trabecular number (Tb. N, 1/mm), and trabecular separation/spacing (Tb.Sp, mm).

2.11. Histology and immunohistochemistry

Histological and immunohistochemical analyses were performed after the completion of micro-CT scanning. Calcein-labeled mouse femurs were fixed in ethanol and dehydrated, and hard tissue sections were made for subsequent observation of calcium salt deposition lines. Femurs from mice in the unlabeled calcein group were decalcified in 10 % EDTA for 21 days. Subsequently, the distal end of the femur was embedded in paraffin and then sectioned at 5 μm using a microtome. The sections were then subjected to immunohistochemical staining with primary antibodies against Traf6 (ab33915, Abcam), Nlrp3 (MA5-32255, Thermo Fisher Scientific, Bothell, WA, USA), and Osx (ab209484, Abcam). Stained sections were photographed using a Confocal microscope (SS-MCS6, Jianzhi instrument equipment, Nanjing, China). Histomorphological analysis of the bones was performed using BIOQUANTOSTEO software (BIOQUANTImageAnalysisCorporation, Nashville, TN, USA).

2.12. Statistical analysis

The experiment was statistically analyzed using SPSS 25.0 software. All experimental data were expressed as mean ± standard deviation (M ± SD). Comparisons between two groups were performed using a *t*-test, and data from multiple groups were compared using one-way analysis of variance. $p < 0.05$ indicated statistically significant differences.

3. Data availability

The data supporting the findings of this study are available from the corresponding author upon request.

4. Results

4.1. Mouse BMSCs derived from the SOP model significantly upregulated senescence indicators and reduced osteogenic differentiation capacity

Scanning of 3-month-old (3Ms) and 18-month-old (18Ms) mice using micro-CT revealed bone loss in senescent mice (Fig. 1A). The bone mineral density of mice in the 18Ms group (0.202 ± 0.035 g/cm^3) was significantly lower than that of mice in the 3Ms group (0.119 ± 0.041 g/cm^3) (Fig. 1B), and there were significant differences in bone microstructure parameters compared with 3Ms group (Fig. 1C–E). Calcein fluorescence labeling showed a significantly lower rate of calcium salt deposition in the distal femur of 18Ms mice than in 3Ms mice (Fig. 1F–G). Next, we isolated and purified primary BMSCs from both age groups, identified them using flow cytometry and microscopy after separation (Fig. S1A–B), and subjected them to beta-galactosidase staining. The results revealed significantly higher galactosidase activity and a greater number of positive cells in the 18Ms group than in the control group (Fig. 1H–K). A cell proliferation assay confirmed that BMSCs derived from 18Ms mice had significantly reduced proliferative capacity compared to those of 3Ms mice (Fig. 1L). ARS and ALP staining after osteogenic induction confirmed that BMSCs from 18Ms mice had significantly lower osteogenic activity than those from 3Ms mice (Fig. 1M−P). WB analysis showed that senescence-associated proteins, p16, p21and p53, were significantly upregulated in BMSCs from the 18Ms group, whereas the expression levels of osteogenesis-associated proteins, Runx2 and Osx, were significantly downregulated (Fig. 1Q–V).

4.2. Differentially expressed genes in BMSCs from senescent mice are enriched in inflammation-related pathways, and Nlrp3 inflammatory vesicles are expressed at significantly higher levels than in BMSCs from young mice

To further explore the factors affecting BMSC aging, we used high-throughput sequencing to screen differentially expressed genes, and Gene Ontology analysis revealed enrichment in immune-inflammation-related functions (Fig. 2A). Kyoto Encyclopedia of Genes and Genomes analysis results showed that BMSCs from 18Ms mice had higher expression of inflammation-related genes, such as TLRs, TNF-α, and NLR, than those from 3Ms mice (Fig. 2C). Further protein-protein interaction network plotting showed correlations among the top 30 differentially expressed genes, including IL-1β and IL-6 (Fig. 2B). Similarly, GSEA confirmed an ES score of 0.350 in the immune response gene set, indicating an upregulated pathway (Fig. 3A). The heat map of the related gene set revealed significant differences in IL-1β and Nlrp3 expression (Fig. 3B). Consequently, we further validated the protein levels of Nlrp3, IL-1β, and IL-18 using WB experiments, which confirmed

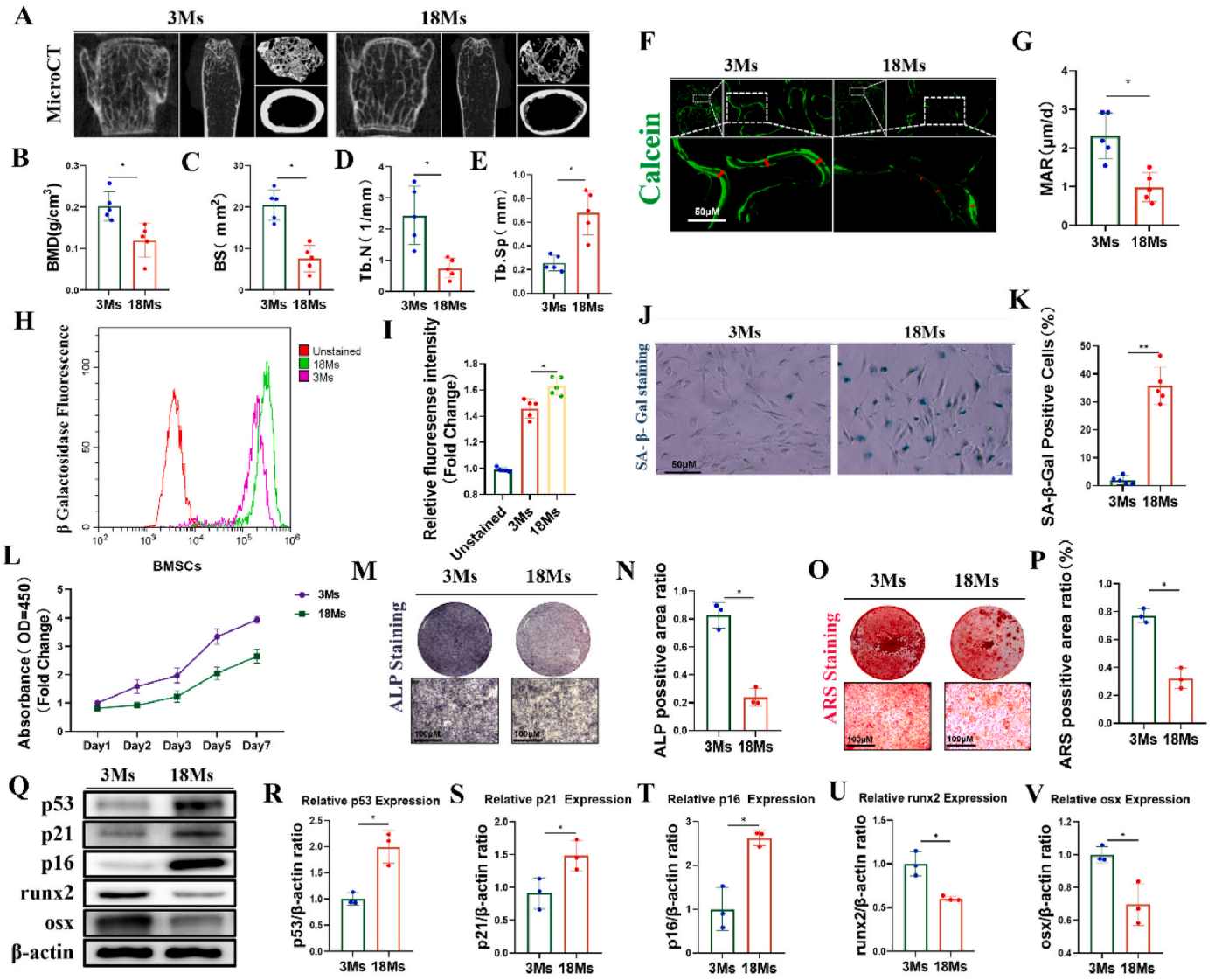

Fig. 1. (A) Micro-computed tomography images of the spine and distal femur in the 3Ms and 18Ms groups. (B–E) Five mice in each group of 3Ms and 18Ms groups were used to analyze the bone mineral density and bone microstructure parameters of the distal femur of each mouse (n = 5, 3Ms group vs. 18Ms group, *P < 0.05) (F–G) Five mice in each group were intraperitoneally injected with calcein 10 days and 3 days before material extraction. Two calcium salt deposition lines were observed after non decalcified hard tissue sections, and the calcium salt deposition rate of the two groups of patients was measured and analyzed. (Calcium salt deposition rate = (the distance between two calcium salt deposition lines)/7d, n = 5, *P < 0.05, scale bar = 50 μm). (H–I) The senescence levels of BMSCs at passage 3 from five mice in each of 3Ms and 18Ms groups were analyzed by flow cytometry. (n = 5, 3Ms group vs. 18Ms group, *P < 0.05). (J–K) Galactose staining was used to detect the senescence level of BMSCs at passage 3 from five mice each from 3Ms to 18Ms groups. (3Ms group vs. 18Ms group, **P < 0.01, n = 5, scale bar = 50 μm). (L) CCK8 assay to detect cell proliferation rate in each group. (n = 3, 3Ms group vs. 18Ms group). (M–P) The osteogenic differentiation ability of BMSCs at passage 3 from 3 mice in 3Ms and 18Ms groups was detected by ALP and ARS staining, and the proportion of staining positive area to the total area was calculated. Three duplicate wells were set up for each sample, and the average value of measurement was taken. (3Ms group vs. 18Ms group, scale bar = 100 μm, n = 3, *P < 0.05). (Q–V) The expression levels of senescence related proteins p16, p21 and p53, as well as osteogenesis related proteins runx2 and osx in BMSCs at passage 3 from three mice in 3Ms and 18Ms groups were detected and quantified by WB experiment. (n = 3, 3Ms group vs. 18Ms group, *P < 0.05).
3Ms, 3-month-old; 18Ms, 18-month-old; BMSCs, bone marrow stromal stem cells.

significant upregulation in senescent BMSCs (Fig. 3C–F). Additionally, we queried GeneCards and OMIM for disease targets related to SOP and inflammatory bone senescence. Using the GSE35958 dataset from the Gene Expression Omnibus (GEO) database, which contains transcriptomic data and clinical information on BMSCs from elderly patients with normal and primary osteoporosis, we identified common differences in inflammation-related genes with crosstalk between Nlrp3, IL-1β, IL-18, Nfe2l2, TRL4, and Traf6 (Fig. 3G and H). Existing literature suggests that Traf6 is closely associated with inflammatory responses and promotes the release of inflammatory cytokines by activating Nlrp3 inflammatory vesicles [15]. Nrf2 negatively correlates with Traf6-related pathway activation during the regulation of inflammation-associated autophagy [16]. Therefore, Traf6 plays a key role in inflammation and Nrf2-associated oxidative stress. Although chronic inflammation and high intracellular oxidative stress levels are closely associated with senescence, the association between the dysregulation of Traf6 expression and progression of inflammatory senescence warrants further investigation.

4.3. Abnormal levels of pro-inflammatory Traf6 and Nrf2 in senescent BMSCs may be closely related to inflammatory senescence progression induced by high levels of inflammation and oxidative stress in BMSCs

Our WB experiments showed significantly increased Traf6 and Nrf2

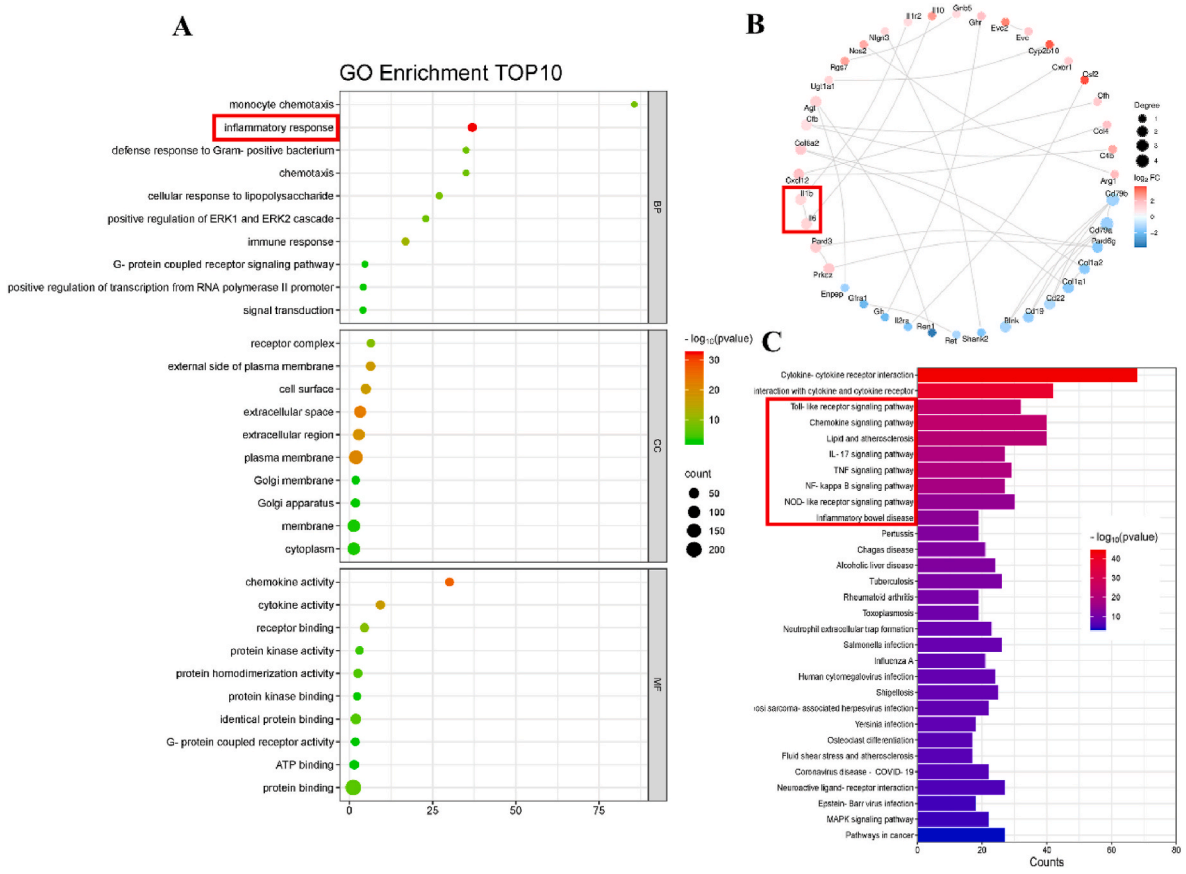

Fig. 2. High-throughput sequencing analysis of differential gene enrichment in inflammation-related pathways. (A) GO analysis of differential gene enrichment. (B) Protein-protein interaction network diagram showing the correlation of the top 30 differentially expressed genes. (C) KEGG analysis of differential gene enrichment in relevant pathways.

expression levels in BMSCs from 18Ms mice (Fig. 4A–C), whereas further detection of intracellular ROS levels in the two groups using Lipid Peroxidation Sensor (ThermoFisher Scientific, D3861) revealed higher levels of oxidative stress in the cells of the 18Ms group (Fig. 4D–E). These findings suggest that BMSC senescence is associated with abnormal intracellular inflammation, oxidative stress, and dysregulated Traf6 and Nrf2 expression. Additionally, we established an inflammatory senescence model of BMSCs using hydrogen peroxide stimulation. BMSCs were treated with 200 μM H_2O_2 for 2 h and then changed to normal medium. After 2 h of 200 μM H_2O_2 treatment, Traf6 and Nlrp3 protein levels were acutely upregulated and remained high within 3 days, whereas Nrf2 expression significantly reduced on day 3. The levels of the senescence-related indicators, p16, p21 and p53, continuously increased (Fig. 4F–L). Subsequent osteogenic induction experiments showed significantly reduced osteogenic function of BMSCs in the inflammatory senescence model (Fig. 4M–Q). These results confirmed the feasibility of H_2O_2 to construct inflammatory senescence models. Aberrant Traf6 expression positively correlated with high inflammation and oxidative stress levels and negatively correlated with Nrf2 expression in senescent cells.

4.4. Targeting Traf6 on BMSCs affects Nrf2 and Nlrp3 expression and regulates intracellular inflammation and oxidative stress levels

To target Traf6 expression, we established a lentiviral transfection model of BMSCs, verified the transfection efficiency through WB, and selected the viral strain with the highest knockdown efficiency (Fig. S2A–D). H_2O_2 induction experiments showed that targeted Traf6 knockdown effectively alleviated the decrease in Nrf2 expression and upregulation of Nlrp3 caused by inflammatory senescence. (Fig. 5A–D). Cytofluorescence experiments confirmed significant upregulation of Nrf2 entry and expression levels (Fig. 5E and F). Further, WB experiments confirmed that targeting Traf6 inhibited the upregulation of inflammatory vesicle-associated proteins, IL-1β and IL-18, and senescence-associated proteins, p16, p21 and p53 (Fig. 5G–I; Fig. 6A–D). Additionally, targeting Traf6 expression effectively reduced the oxidative stress level in BMSC cells. (Fig. 5J–K), alleviated the decline in osteogenic function caused by inflammatory senescence (Fig. 6G–N), and inhibited their differentiation into adipocytes (Fig. 6O and P).

4.5. The Traf6/Nrf2/Nlrp3 signaling pathway has a major impact on senescence progression and loss of osteogenic capacity in BMSCs

Next, we verified that Traf6 regulates inflammatory senescence progression via Nrf2/Nlrp3 using an Nrf2 agonist (TBHQ) and inhibitor (ML385). CCK8 experiments determined that the maximum non-toxic concentrations of TBHQ and ML385 were 10 μM and 1 μM, respectively (Fig. S2E–F). In subsequent rescue intervention experiments, Nrf2 agonism effectively inhibited the upregulation of inflammatory vesicle proteins, Nlrp3, IL-1β, and IL-18, and attenuated oxidative stress-induced inflammatory senescence progression. Furthermore, the beneficial effect of targeted Traf6 knockdown in attenuating senescence progression was reversed through Nrf2 inhibition (Fig. 7A–D). Osteogenic induction experiments showed that the expression of the osteogenesis-related proteins, Runx2 and Osx, was negatively correlated with inflammatory senescence progression and could be rescued through Nrf2 intervention in the same batch of identically treated BMSCs on day 3 of induction (Fig. 7E–I). These findings indicate that Nrf2 plays an important role in the link between Traf6, inflammatory oxidative stress, and senescence progression.

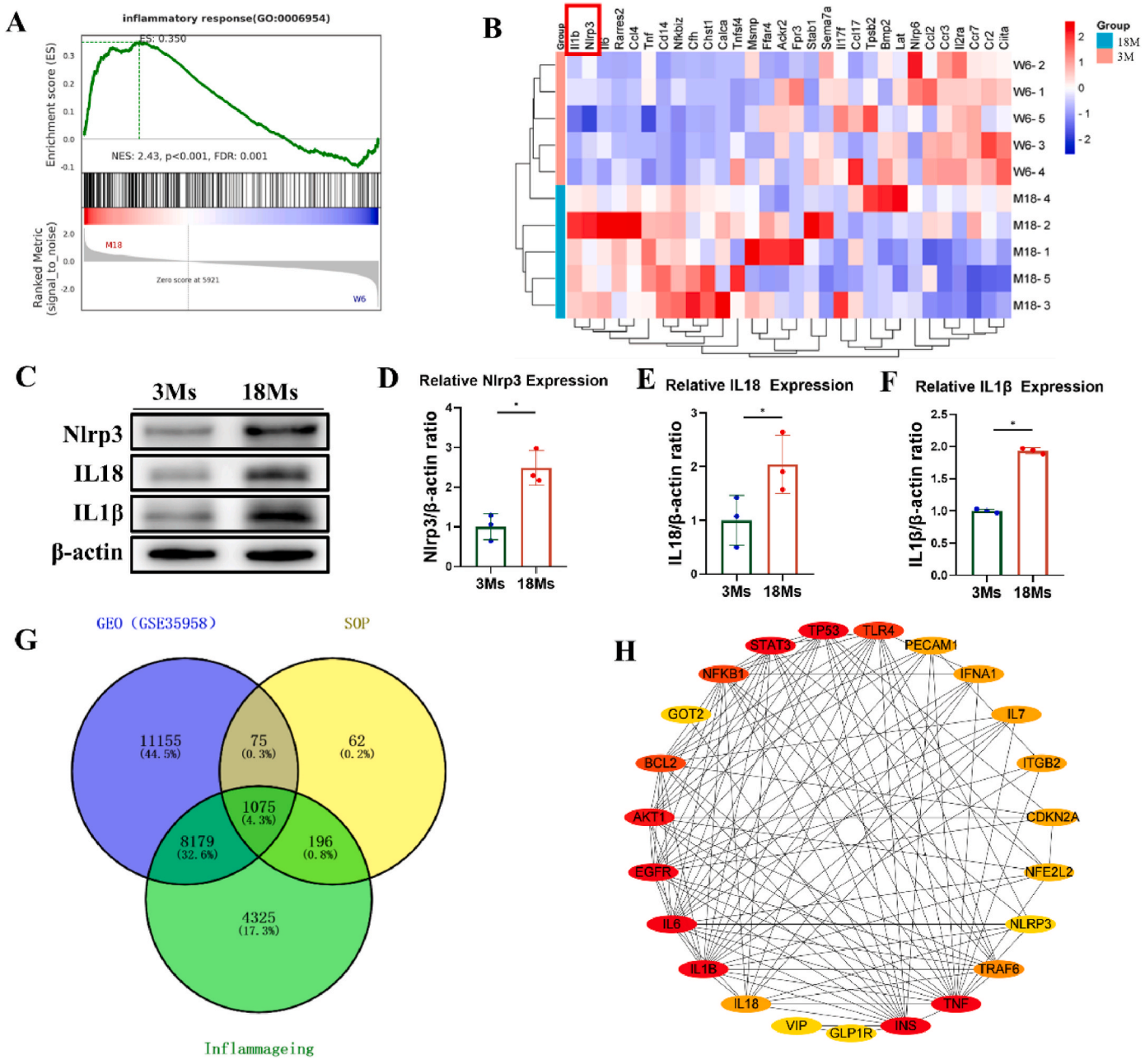

Fig. 3. Differential upregulation of genes enriched in inflammation-related pathways in the 18Ms group compared to in the 3Ms group. (A) GSEA analysis showing the enriched pathway. (B) Heatmap showing inflammation-related differential gene sets. (C–F) The expression levels of Nirp3, IL-18 and IL-1β in BMSCs at passage 3 from three mice in the 3Ms and 18Ms groups were detected and quantified by WB experiment. (3Ms group vs. 18Ms group, n = 3, *P < 0.05). (G) Wayne's plots showing SOPs obtained from GeneCards and OMIM query, disease targets associated with inflammatory bone aging, and datasets in the Gene Expression Omnibus (GEO) database GSE35958 related genes. (H) PPI network plot showing the correlation of commonly differentially expressed inflammation-related genes.
3Ms, 3-month-old; 18Ms, 18-month-old; PPI, protein-protein interaction; WB, Western blot.

4.6. Targeted knockdown of Traf6 in bone tissue affects Nlrp3 expression and reduces inflammation and oxidative stress levels

In the in vivo experiments, we used a lentiviral intratumoral injection to deliver a high concentration of shtraf6 viral fluid to target bone tissue transfection. Two weeks post-transfection, bone marrow cells from transfected mice were extracted, and after the cells were wall-adhered and purified by isolation, fluorescence microscopy showed a GFP positivity rate of up to 45 %. Subsequent WB confirmed that the lentiviral bone marrow intratumoral injection achieved good transfection and knockdown efficiencies (Fig. S2G–J). After determining the transfection efficiency, a similar batch of shtraf6 group mice was injected with galactose (150 mg/kg/day) for 8 weeks to induce a subacute senescence model. Immunohistochemical results showed that Traf6-positive OID around the bone trabeculae was significantly 1.88 times higher in the senescence model group than in the control group; however, it significantly reduced to 51 % in the lentiviral transfection group (Fig. S3A–B). Meanwhile, the expression level of P53 in the model group significantly increased, while targeted knockdown of Traf6 effectively inhibited D-galactose-induced aging progression (Fig. S3C–D). Additionally, the number of adipocytes in the senescence model group significantly increased, and targeted Traf6 knockdown significantly reduced adipocyte content in bone marrow tissue. This result was consistent with that of our in vitro experiments, which

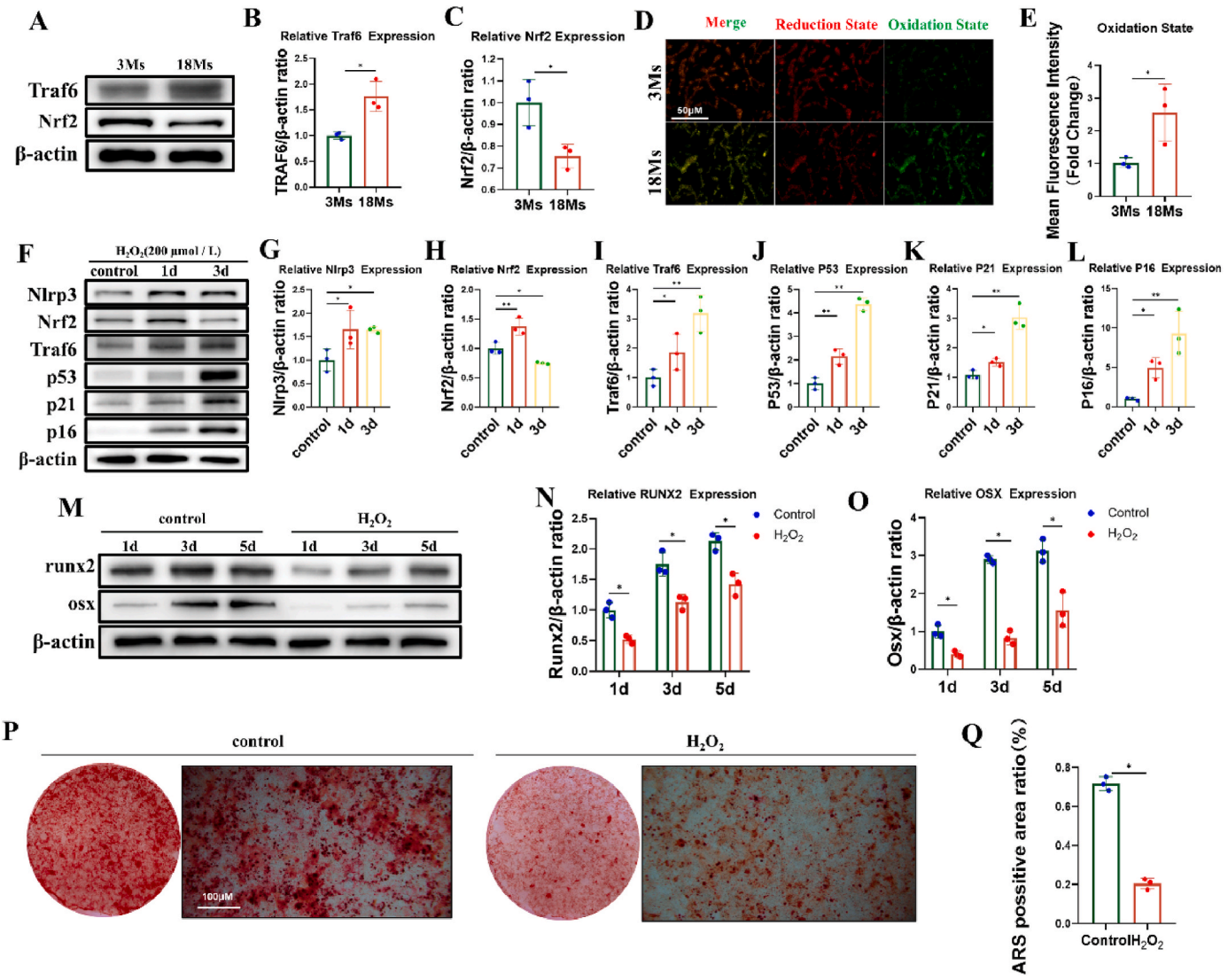

Fig. 4. Upregulated oxidative stress level and decreased osteogenic function in the 18Ms group compared with in the 3Ms group. (A–C) WB experiments were used to verify the expression levels of Traf6 and Nrf2 in BMSCs at passage 3 from 3 mice in each of the 3Ms and 18Ms groups, and the related indicators were quantitatively analyzed. (n = 3, 3Ms group vs. 18Ms group, *P < 0.05). (D–E) Detection of intracellular reactive oxygen species levels with undecanoic acid in above both groups. (n = 3, 3Ms group vs. 18Ms group, *P < 0.05). (F–L) BMSCs at passage 3 from 3Ms mice were seeded into 6-well plates at a density of 1×10^5 cells/well. After intervention with 200 μ mol/L H_2O_2, the expression of senescence and oxidative stress-related proteins and quantitative analysis of related indicators were detected by WB experiment. The experiment was repeated three times, and BMSCs from different mouse sources were selected for each experiment. (n = 3, *P < 0.05, **P < 0.01). (M–O) After H_2O_2 induced senescence of BMSCs for 3 days, WB experiments verified that the expression levels of osteogenesis related proteins runx2 and osx were significantly lower than those of the control group on the 1st, 3rd and 5th day of osteogenesis induction. The experiment was repeated three times, and BMSCs from different mouse sources were selected for each experiment. (n = 3, control group vs. H_2O_2 group, *P < 0.05, **P < 0.01). (P–Q) ARS staining showing the bone differentiation ability of the above two groups, and the proportion of staining positive area to the total area was calculated. (n = 3, control group vs. H_2O_2 group, *P < 0.05).
3Ms, 3-month-old; 18Ms, 18-month-old.

involved targeting Traf6 and inducing adipogenic differentiation (Fig. S3E). Further immunofluorescence staining and serum ELISA results showed that the following were significantly increased in bone tissue in the aging model: Nlrp3, serum inflammatory factors IL-1β and IL-6, and lipid peroxidation product MDA levels (Fig. 8A–B, E-F; Fig. S3F). This increase was negatively correlated with the expression of OSX and OCN (Osteocalcin) and could be reversed by targeted Traf6 knockdown (Fig. 8C–D, G).

4.7. Targeted Traf6 knockdown in bone tissue reduces SOP progression

Micro-CT results showed that the BMD in the shtraf6 mouse group was significantly higher than that in the model group, with significantly improved bone microstructural parameters (BMD in mg/mm^3: 0.18 ± 0.01 vs. 0.13 ± 0.01, BS in mm^2: 13.13 ± 1.50 vs. 6.49 ± 2.91, BV/TV in %: 10.97 ± 0.92 vs. 5.53 ± 1.83, Tb.Th in mm: 0.92 vs. 5.53 ± 1.83, Tb.Sp in mm: 0.288 ± 0.06 vs. 0.53 ± 0.30, Tb.N in 1/mm: 1.60 ± 0.10 vs. 0.77 ± 0.35) (Fig. 9A–F). Von Kossa staining showed that the area of bone trabeculae was negatively correlated with Traf6 expression (Fig. 9G and H). Calcein labeling showed that the rate of calcium salt deposition in senescent mice was 0.51 ± 0.25 μm/d, which was significantly lower than that in the control group (2.41 ± 0.42 μm/d), whereas the calcium salt deposition rate reached 1.63 ± 0.41 μm/d in the shtraf6 group (Fig. 9I and J). These results confirmed that Traf6 expression in bone tissue was positively correlated with inflammation and SOP progression and that intervention targeting Traf6 expression

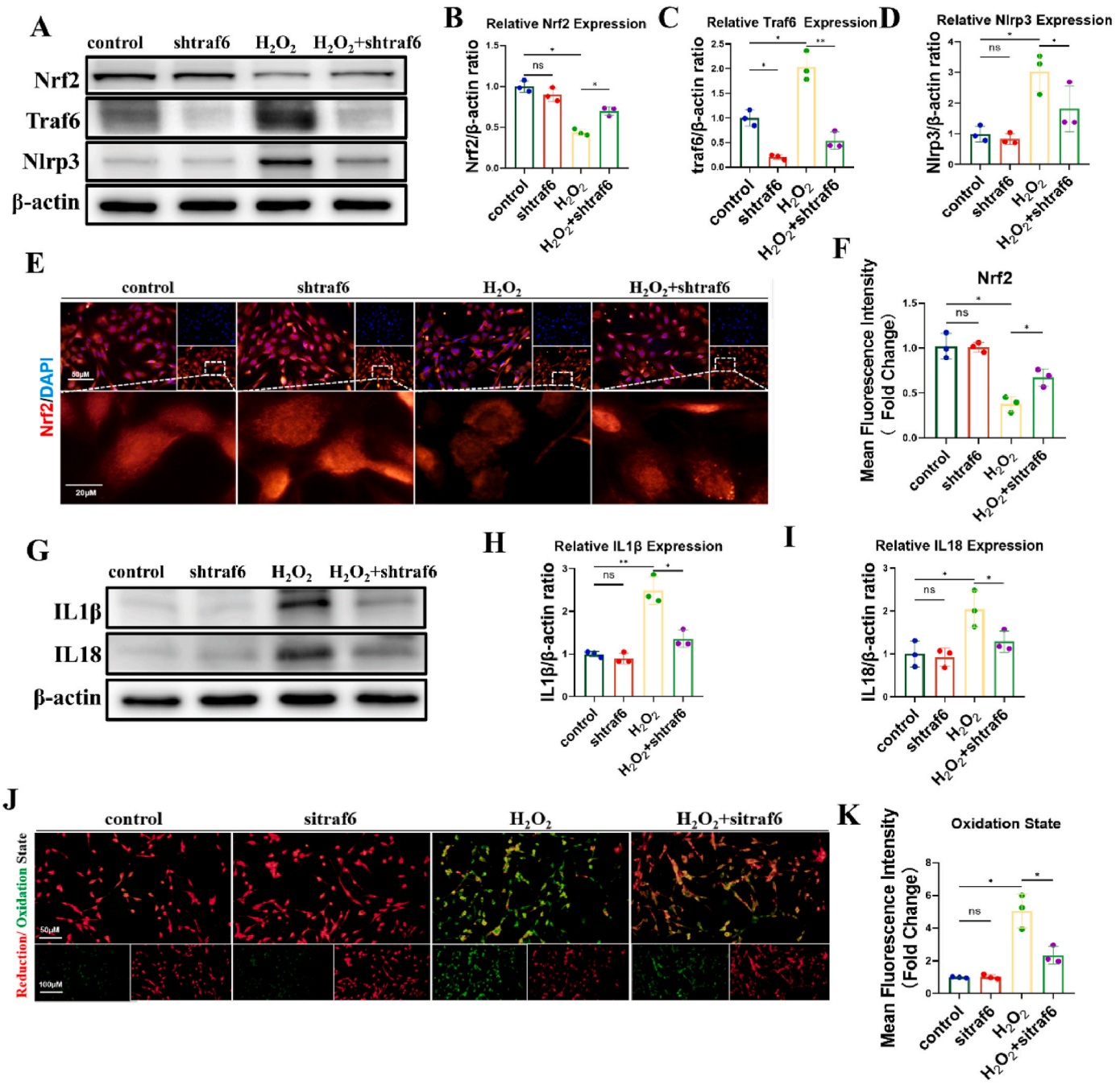

Fig. 5. Effective inhibition of the expression of Nlrp3 inflammatory vesicles through lentiviral knockdown of Traf6. (A–D) BMSCs at passage 3 and LV-shtraf6 transfected cells from 3Ms mice were seeded into 6-well plates at a density of 1×10^5 cells/well. After intervention with 200 μ mol/L H_2O_2, the expression of Traf6, Nrf2 and Nlrp3 were detected by WB experiment. The experiment was repeated three times, and BMSCs from different mouse sources were selected for each experiment. (n = 3, *P < 0.05, **P < 0.01, ns: No significance). (E–F) Immunofluorescence staining showing the expression and nucleation level of Nrf2 in above each group, and the fluorescence intensity of Nrf2 was quantified (n = 3, *P < 0.05, **P < 0.01, ns: No significance). (G–I) Western blot images showing the expression levels of inflammatory vesicle component proteins, IL-18 and IL-1β, in above each group (n = 3, *P < 0.05, **P < 0.01, ns: No significance). (J–K) Undecanoic acid detection of intracellular oxidative stress levels in each group, and the level of oxidative stress in above each group was quantified. (n = 3, *P < 0.05, **P < 0.01, ns: No significance).

can effectively alleviate osteoporosis progression caused by inflammatory senescence.

5. Discussion

The progression of senescence in BMSCs in the bone homeostatic microenvironment is accompanied by decreased proliferative and differentiation capacity and abnormalities in stem cell biology [9]. Researchers have also confirmed that inflammation and oxidative stress-mediated inflammatory senescence significantly contribute to the development and progression of osteoporosis in the elderly [17]. Inflammatory senescence refers to a state of long-term chronic pro-inflammatory response that progressively increases with senescence and is closely associated with the development of various age-related diseases [18]. Our previous high-throughput sequencing analysis confirmed that genes differentially expressed in senescent BMSCs were

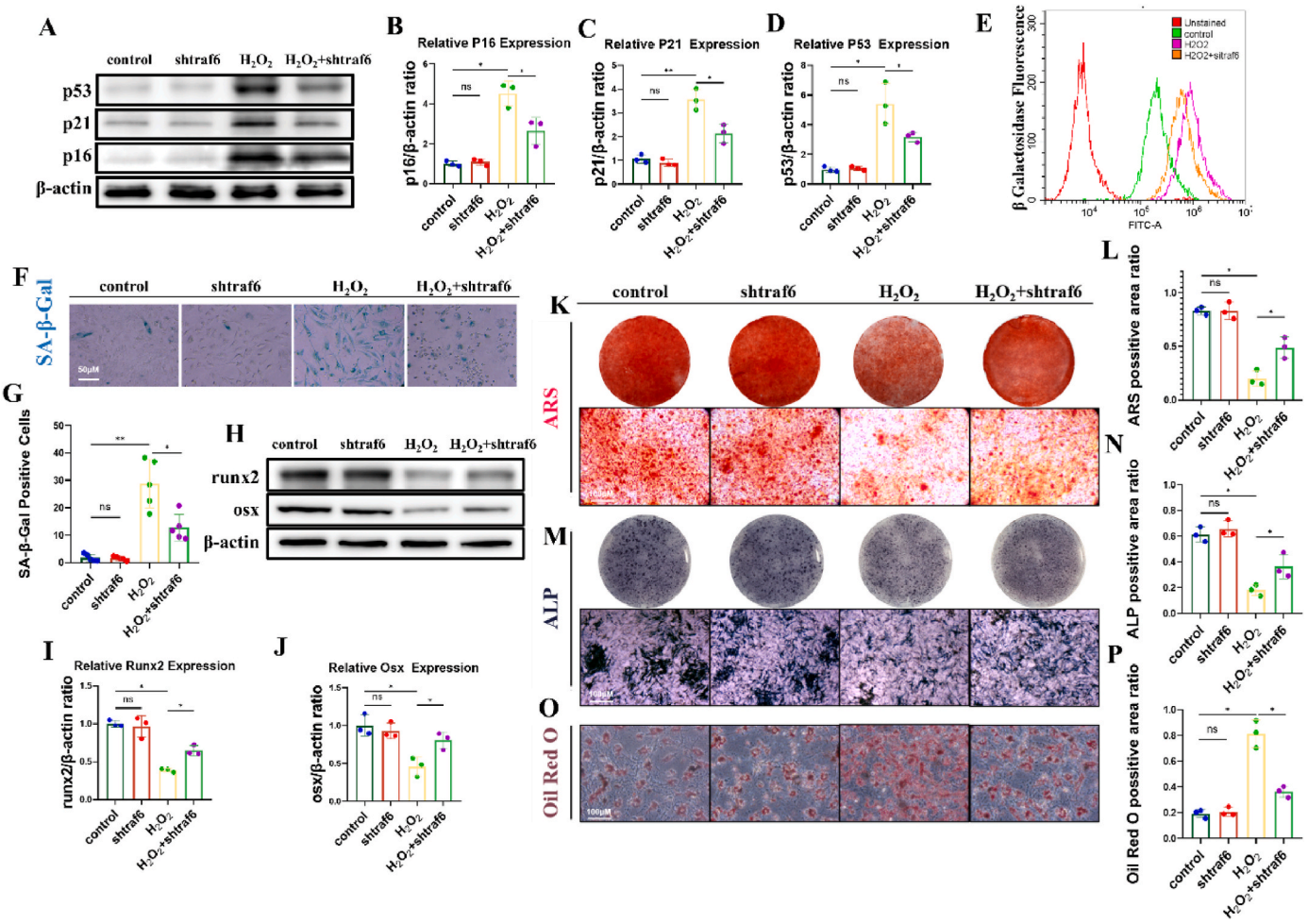

Fig. 6. Targeted knockdown of Traf6 delays the progression of inflammatory senescence in BMSCs and alleviates the decline in osteogenic function caused by inflammatory senescence. (A–D) BMSCs at passage 3 and LV-shtraf6 transfected cells from 3Ms mice were seeded into 6-well plates at a density of 1×10^5 cells/well. After intervention with 200 μ mol/L H_2O_2 for 3d, the expression of p16, p21 and p53 were detected by WB experiment. The experiment was repeated three times, and BMSCs from different mouse sources were selected for each experiment. (n = 3, *P < 0.05, **P < 0.01, ns: No significance). (E–G) Flow cytometry and galactose staining showing the level of cellular senescence in above each group. (H–J) Typical WB images showed the expression of osteogenic related proteins in the above groups of cells after osteogenic induction for 5 days. Quantitative analysis results showed that targeted intervention of TRAF6 could effectively reduce the decline of osteogenic function caused by inflammation and senescence. The experiment was repeated three times, and BMSCs from different mouse sources were selected for each experiment. (n = 3, *P < 0.05, **P < 0.01, ns: No significance). (K–P) BMSCs at passage 3 and LV-shtraf6 transfected cells from 3Ms mice were seeded into 6-well plates at a density of 1×10^5 cells/well. After intervention with 200 μ mol/L H_2O_2, ARS and ALP staining were performed after osteogenesis induction, and oil red staining was performed after lipogenesis induction, and the proportion of staining positive area to the total area was calculated. The experiment was repeated three times, and BMSCs from different 3Ms mouse sources were selected for each experiment. (n = 3, *P < 0.05, **P < 0.01, ns: No significance).
BMSCs, bone marrow stromal stem cells.

highly enriched in inflammatory and oxidative stress-related pathways. To further explore the regulatory mechanisms affecting intracellular inflammation and oxidative stress levels in BMSCs, we searched the GeneCards and OMIM databases for SOP using the search terms “senile osteoporosis” and “inflammatory bone aging” and obtained the GSE dataset. We obtained the GSE35958 dataset from the GEO database, which contains transcriptomics and clinical data of BMSCs from elderly patients with normal and primary osteoporosis. Wayne’s and protein-protein interaction visual network diagrams indicated close associations among Traf6, Nrf2, and Nlrp3, suggesting their significant roles in the progression of inflammatory senescence in BMSCs. Furthermore, our additional in vitro and in vivo experiments confirmed that targeting Traf6 could modulate Nrf2/Nlrp3 to delay the progression of inflammatory senescence in BMSCs.

Several studies have shown that Traf6 is closely associated with organismal senescence, is sensitive to inflammation, and plays an important role in innate and acquired immunity, bone metabolism, and other systems [19,20]. In this study, we also observed that the reduction of Nrf2 protein levels in senescent BMSCs could be reversed by targeted knockdown of Traf6. Nrf2, as an endogenous antioxidant stress factor, regulates oxidative stress in organisms [21]. Under physiological conditions, Nrf2 binds to the negative regulator, Keap1, in the cytosol, where it undergoes ubiquitination and degradation by the 26S protease; this maintains Nrf2 at low basal levels. Upon external stimulation, Keap1 uncouples from Nrf2, allowing Nrf2 to translocate into the nucleus, bind to antioxidant response elements, and activate downstream target genes that maintain intracellular redox homeostasis, thereby exerting endogenous protective effects [22]. However, as an important transcription factor for cellular antioxidant and anti-chemical damage, Nrf2 has been found to have a complex crosstalk with NF-κB, MAPK, and other signaling pathways. Previous studies have confirmed that Nrf2 can reduce the levels of reactive oxygen radicals in the cell by inducing the expression of antioxidant enzymes, thereby affecting the NF-κB and MAPK pathways [23–25]. The Nfe2l2 promoter also has a binding site for p65, which binds to it and activates its transcription when phosphorylated in the nucleus [26]. The specific intervention with ERK can

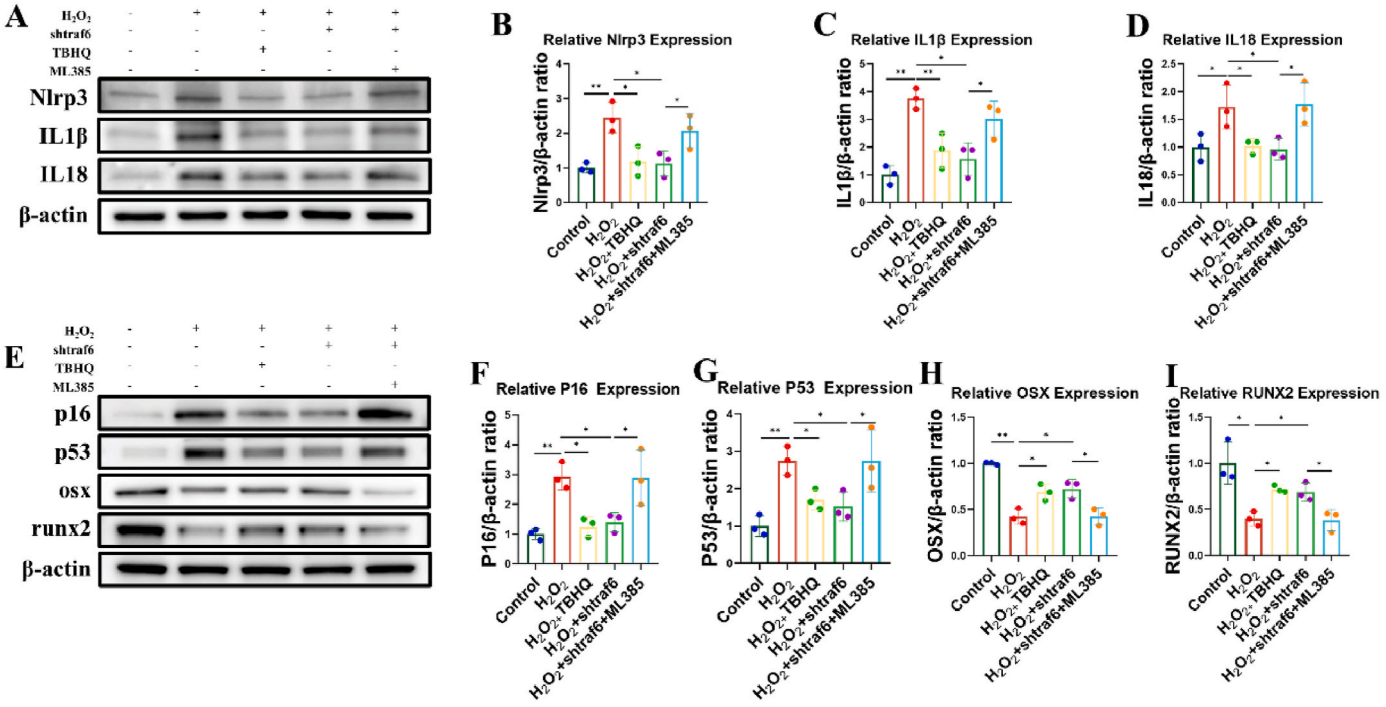

Fig. 7. Traf6/Nrf2 is an important regulator of Nlrp3 inflammatory vesicle protein expression. (A–D) Typical WB images showed that Nrf2 agonist (TBHQ) inhibited the H_2O_2 induced upregulation of Nlrp3, IL-18 and IL-1β expression levels, and the inhibitory effect of the expression of inflammasome after targeted knockdown of Traf6 was also reversed by the intervention of Nrf2 inhibitor (ML385). The experiment was repeated three times, and BMSCs from different 3Ms mouse sources were selected for each experiment. (n = 3, *P < 0.05, **P < 0.01). (E–I) The typical WB images showed the expression of p16, p53, runx2 and osx in the above groups. The quantitative analysis results showed that the targeted knockdown of Traf6, the intervention of Nrf2 agonists and inhibitors on the expression of aging and osteogenesis related proteins. The experiment was repeated three times, and BMSCs from different 3Ms mouse sources were selected for each experiment. (n = 3, *P < 0.05, **P < 0.01).

affect the recognition and binding of Nrf2 to the ARE, which regulates a number of downstream oxidative and chemical damage signaling pathways. ARE regulates the expression of a number of downstream genes that protect against oxidative stress [27].

Studies have shown that the NF-κB and MAPK pathways are also closely linked to cellular inflammation and oxidative stress. Chen et al. found that the transcription factor, p65, was aberrantly activated in osteoblasts and osteoclasts of prematurely aging ERCC1-XPF-deficient mice [28]. Furthermore, Widjaja et al. demonstrated that intervention targeting the expression of the inflammatory factor, IL-11, could modulate the ERK pathway, leading to a decrease in downstream AMPK activity and slowing the process of cellular senescence [29]. Additionally, Melough et al. also suggested that oxidative stress is an important pathological trigger for SOP progression and that upregulation of signaling pathways, such as the JNK/p38 MAPK pathway, is an important regulatory mechanism for age-related bone loss [30]. Our additional experiments also revealed that the abnormal reduction of Nrf2 expression levels in senescent BMSCs was indeed accompanied by an abnormal upregulation of phosphorylation levels of p65, ERK, JNK, and p38. After the intervention targeting Traf6 expression, the phosphorylation levels of p65, ERK, p38, and JNK were also significantly downregulated, whereas Nrf2/Nlrp3 was regulated to influence the progression of inflammatory senescence in BMSCs (Fig. S5). It can be concluded that Traf6-targeted intervention can regulate NF-κB and MAPK and directly or indirectly affect the Nrf2/Nlrp3 signaling axis, which is an effective means to delay the progression of inflammatory senescence in BMSCs.

In our in vivo experiments, ELISA results revealed elevated inflammatory factor levels in SOP mouse serum, alongside significantly reduced expression of osteogenesis-related markers. Immunofluorescence staining of bone tissue also confirmed significantly increased Nlrp3 protein levels in the senescent bone microenvironment. He et al. confirmed that dysregulation of Nlrp3 inflammasome expression induces age-associated chronic inflammation and highlighted that targeted inhibition of Nlrp3 inflammasome activation could slow the progression of inflammatory senescence [31]. In contrast, after high-concentration lentiviral knockdown of Traf6 via an isovolumic injection into the bone marrow cavity, serum inflammation levels and Nlrp3 expression in bone tissue were significantly suppressed in the intervention group. Moreover, bone volume and calcium salt deposition in the distal femur were significantly higher in mice in the intervention group than in mice in the senescent model group. Similar to cellular experiments, targeted Traf6 intervention in vivo effectively reduces Nlrp3 expression, suppresses inflammation levels, and alleviates SOP progression. Additionally, inflammation levels in bone tissue are closely associated with immune-related cells and BMMs. Our previous study confirmed that NF-κB (a downstream pathway of Traf6) intervention can inhibit the abnormal activation of osteoclasts [32]. In this study, we found that serum CTX-1 levels and the number of Trap-positive cells were significantly lower in the intervention group than in the senescence model group (Fig. S4H–I). Deepak et al. found that targeting Traf6 protein stabilization in the intramedullary region inhibits osteoclast activation and alleviates bone loss [33]. In addition, Wu et al. demonstrated that WDFY3, a major regulator of selective autophagy, interacts with Traf6 and affects RANKL-induced osteoclastogenesis in vitro and in vivo via the NF-κB pathway and further influences the progression of inflammatory arthritis [34,35]. It is evident that targeted intervention of Traf6 can effectively regulate osteoclast activation and affect the level of inflammation in the bone microenvironment. We further validated the efficacy of lentiviral transfection of BMMs in vitro. We found that the LV-shtraf6 viral strain could also effectively transfect BMMs (Fig. S4A–C), and intervention targeting Traf6 could significantly inhibit RANKL-induced differentiation of BMMs into osteoblasts (Fig. S4D–G). It can be seen that the Traf6-targeted intervention can achieve the effect

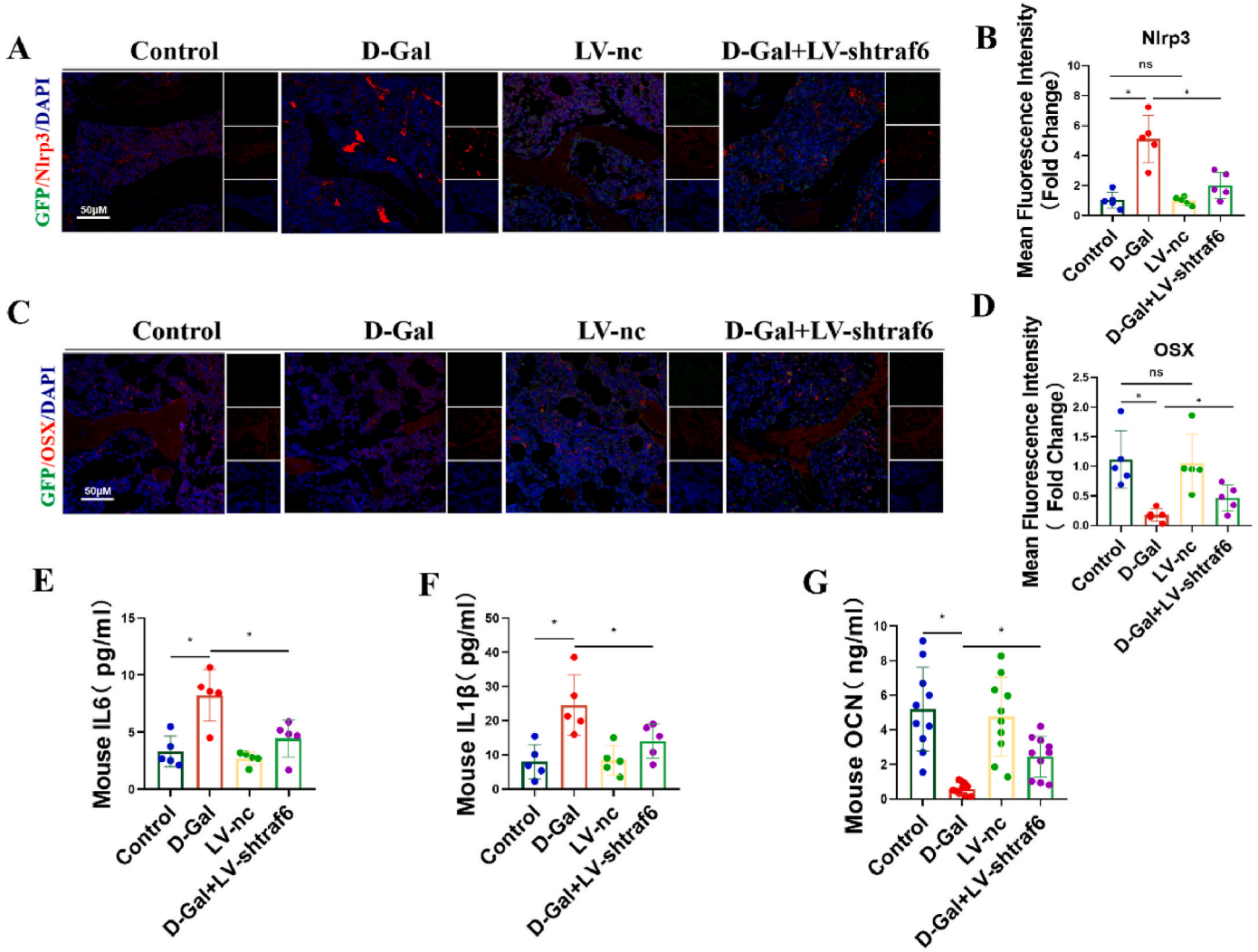

Fig. 8. Targeted knockdown of Traf6 effectively reduces the level of inflammation in bone tissue and alleviates the age-related decline in osteogenic capacity of BMSCs. (A–D) Immunofluorescence staining was performed on sections of distal femur of 5 mice, the typical immunofluorescence staining images showed the expression of Nlrp3 and osx in bone tissues of each group. Three visual fields were randomly selected from each section to measure the fluorescence intensity, and the average value was taken. The relative fluorescence intensity of Nlrp3 and osx was quantitatively analyzed. (n = 5, *P < 0.05, **P < 0.01, ns: No significance). (E–F) ELISA results showing the serum levels of inflammatory factors, IL-6 and IL-1β in mice of each group, there were 5 mice in each group, and 3 duplicate wells were set up for each independent sample. (n = 5, *P < 0.05). (G) ELISA results showing the serum levels of OCN in mice of each group, there were 10 mice in each group, and 3 duplicate wells were set up for each independent sample. (n = 10, *P < 0.05).
BMSCs, bone marrow stromal stem cells; ELISA, enzyme-linked immunosorbent assay.

of regulating osteogenesis and osteoclastogenesis at the same time.

Existing anti-osteoporosis strategies include the administration of calcium and the use of pharmaceuticals such as teriparatide and denosumab. Moreover, recent clinical trials have demonstrated the efficacy of senolytic therapy in promoting osteogenesis. however, its capacity to inhibit osteoclast activity is limited [36]. Interestingly, intervention targeting Traf6 allows the simultaneous modulation of osteogenesis and osteoclast function. Targeted intervention of Traf6 with safe and effective drugs in bone tissue may be another potential treatment method for SOP besides senolytic therapy. Studies have shown that, salidroside, the natural alkaloid (−)-N-hydroxyapiosporamide, and other natural compounds derived from Chinese herbal medicines exerted significant inhibitory effects on Traf6 [37,38]. These natural compounds have been reported to be effective in inhibiting inflammation and modulating cellular activity in the fields of respiratory disease and anti-tumor treatments. The efficacy of similar natural compounds that can be targeted to inhibit Traf6-related therapeutic effects in the treatment of osteoporosis warrants further investigation. However, most drugs lack target specificity and do not specifically recognize bone tissue, leading to significant accumulation in organs, such as the liver and kidney, resulting in toxic side effects. Therefore, how to achieve targeted drug delivery of natural Traf6 inhibitors within bone tissue requires in-depth study. Recent developments in nanotechnology have made drug delivery more efficient and precise. Currently, several types of nanocarriers are used for the treatment of OP, including lipid carriers [39], exo [40], and various synthetic nanoparticles [41]. Therefore, targeted drug delivery to bone tissue can be achieved by assembling anti-OP drugs with the above carriers. The use of Traf6-targeted interventional drugs by targeted delivery to bone tissue through the assembly of nanocomposites is promising for the treatment of SOP.

While our study provides new insights into the relationship between inflammatory senescence, oxidative stress in BMSCs and SOP. However, there are still limitations to consider. Although salidroside and other natural compounds derived from Chinese herbal medicines exhibit significant inhibitory effects on Traf6, this study did not further intervene with the above-mentioned related drugs in vivo and in vitro to observe the efficacy of drug intervention in Traf6-targeted treatment of SOP. Additionally, this study only detected the relevant histological changes

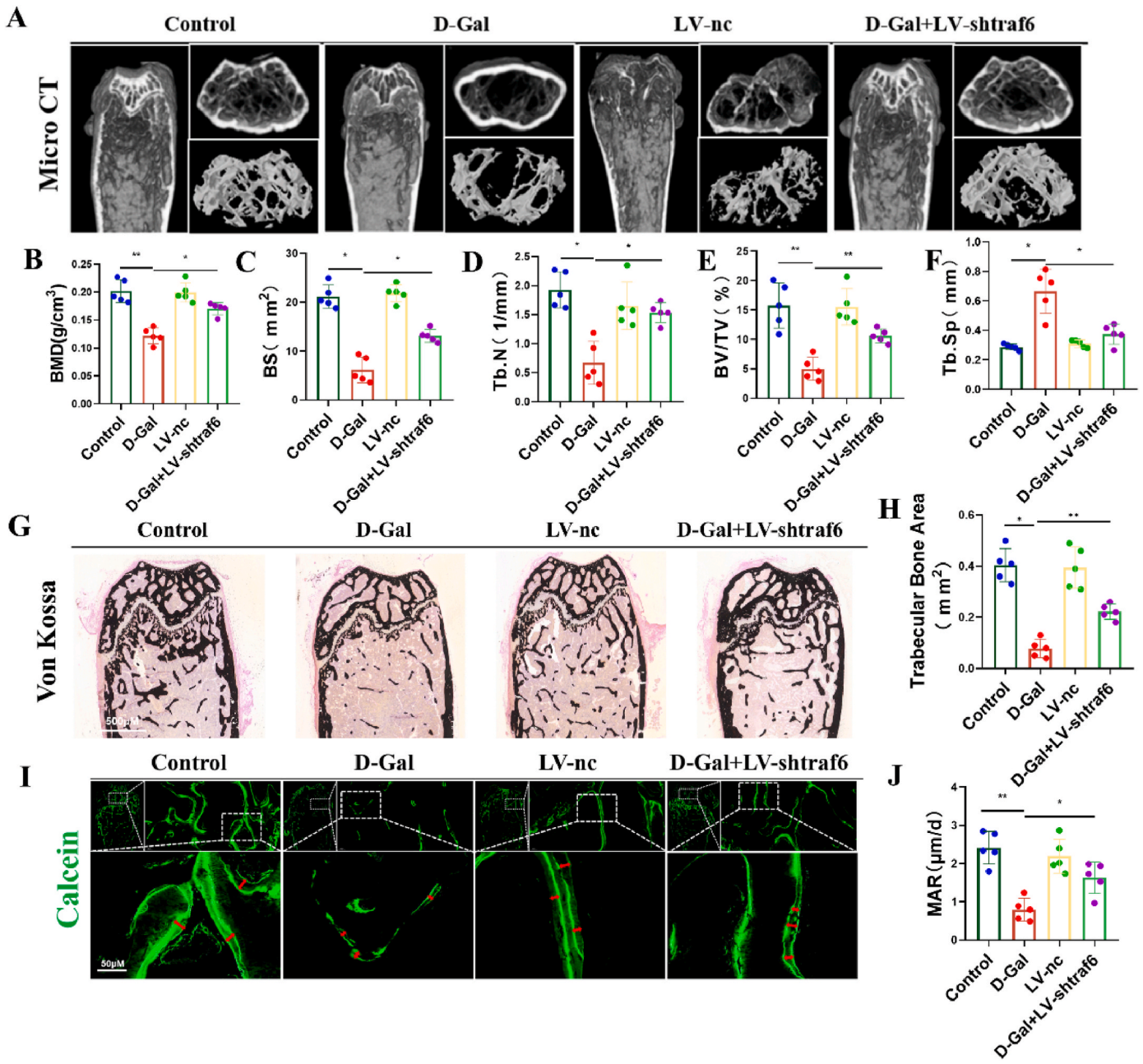

Fig. 9. Targeted knockdown of Traf6 in bone tissue effectively attenuates age-related bone loss. (A–F) Representative 3D microCT images showed the bone microstructure of the distal femur of mice in each group. Five mice in each group were used to analyze the bone mineral density and bone microstructure parameters of the distal femur of each mouse. (n = 5, *P < 0.05, **P < 0.01). (G–H) Von Kossa staining showing the area of distal femoral trabeculae in each group (n = 5, *P < 0.05, **P < 0.01). (I–J) Five mice in each group were intraperitoneally injected with calcein 10 days and 3 days before material extraction. Two calcium salt deposition lines were observed after non decalcified hard tissue sections, and the calcium salt deposition rate of the four groups of patients was measured and analyzed. (Calcium salt deposition rate = (the distance between two calcium salt deposition lines)/7d, n = 5, *P < 0.05, **P < 0.01, scale bar = 50 μm).
CT, computed tomography.

in bone tissue at 8 weeks after targeted knockdown of Traf6, without conducting long-term observations to further clarify the safety and efficacy of Traf6-targeted intervention for SOP treatment. How to achieve targeted delivery of Traf6 inhibitory drugs in bone tissue and conduct long-term observations of their therapeutic effects on SOP warrant further investigation.

In conclusion, the Traf6-mediated Nrf2/Nlrp3 signaling axis significantly influences inflammatory senescence progression in BMSCs. Targeting Traf6 can effectively alleviate the accelerated senescence and decreased osteogenic capacity of BMSCs caused by chronic inflammation, potentially serving as an effective strategy to prevent and control SOP progression.

CRediT authorship contribution statement

Yajun Li: Writing – review & editing, Writing – original draft, Validation, Supervision, Resources, Project administration, Methodology, Funding acquisition, Formal analysis, Data curation, Conceptualization. **Yunshang Yang:** Methodology, Formal analysis, Data curation. **Donglong Xia:** Software, Methodology, Data curation. **Yiling Fang:** Methodology, Investigation, Formal analysis. **Cheng Tang:** Methodology, Investigation. **Jingxian Yu:** Methodology, Data curation. **Dechun**

Geng: Writing – review & editing, Funding acquisition, Formal analysis, Data curation, Conceptualization. **Zhirong Wang:** Project administration, Methodology, Investigation, Funding acquisition, Formal analysis, Data curation, Conceptualization. **Long Xiao:** Resources, Project administration, Methodology, Investigation, Funding acquisition, Formal analysis, Data curation, Conceptualization.

Declaration of competing interest

The authors declare that they have no known competing financial interests or personal relationships that could have appeared to influence the work reported in this paper.

Acknowledgments

This research was financially supported by the National Nature Science Foundation of China (82104892, 82305038), Suzhou Science and Technology Development Plan Project (SYWD2024049, SKY2023079, SYW2025027, SYSD2021175, SKY2021001, SKJY2021002 and SKY2023081). the Key Disciplines in Suzhou (SZXK202120, LCZX202221 and LCZX202331), Natural Science Foundation project of Nanjing University of Traditional Chinese Medicine (XZR2023029), Priority Academic Program Development of Jiangsu Higher Education Institutions (PAPD).

Appendix A. Supplementary data

Supplementary data to this article can be found online at https://doi.org/10.1016/j.redox.2025.103804.

Data availability

Data will be made available on request.

References

[1] B. Uyar, D. Palmer, A. Kowald, et al., Single-cell analyses of aging, inflammation and senescence, Ageing Res. Rev. 64 (2020) 101156.
[2] S. Paik, J.K. Kim, P. Silwal, C. Sasakawa, E.K. Jo, An update on the regulatory mechanisms of NLRP3 inflammasome activation, Cell. Mol. Immunol. 18 (5) (2021) 1141–1160.
[3] Q. Ma, Pharmacological inhibition of the NLRP3 inflammasome: structure, molecular activation, and inhibitor-NLRP3 interaction, Pharmacol. Rev. 75 (3) (2023) 487–520.
[4] H. Xian, K. Watari, E. Sanchez-Lopez, et al., Oxidized DNA fragments exit mitochondria via mPTP- and VDAC-dependent channels to activate NLRP3 inflammasome and interferon signaling, Immunity 55 (8) (2022) 1370–1385, e1378.
[5] J. Li, X. Yi, Z. Yao, J.V. Chakkalakal, L. Xing, B.F. Boyce, TNF receptor-associated factor 6 mediates TNFα-induced skeletal muscle atrophy in mice during aging, J. Bone Miner. Res. : Off. J. Am. Soc. Bone Mineral Res. 35 (8) (2020) 1535–1548.
[6] M. George, M. Tharakan, J. Culberson, A.P. Reddy, P.H. Reddy, Role of Nrf2 in aging, Alzheimer's and other neurodegenerative diseases, Ageing Res. Rev. 82 (2022) 101756.
[7] P. Zhang, Y. Jin, W. Xia, X. Wang, Z. Zhou, Phillygenin inhibits inflammation in chondrocytes via the Nrf2/NF-κB axis and ameliorates osteoarthritis in mice, J. Orthopaedic Translat. 41 (2023) 1–11.
[8] P. Wang, T. Li, C. Niu, S. Sun, D. Liu, ROS-activated MAPK/ERK pathway regulates crosstalk between Nrf2 and Hif-1α to promote IL-17D expression protecting the intestinal epithelial barrier under hyperoxia, Int. Immunopharmacol. 116 (2023) 109763.
[9] F. Liu, Y. Yuan, L. Bai, et al., LRRc17 controls BMSC senescence via mitophagy and inhibits the therapeutic effect of BMSCs on ovariectomy-induced bone loss, Redox Biol. 43 (2021) 101963.
[10] Arifin WN, Zahiruddin WM. Sample size calculation in animal studies using resource equation appr oach. Malays. J. Med. Sci.24(5):101-105.
[11] Z. Liu, H. Wang, Y. Hou, et al., CNC-bZIP protein NFE2L1 regulates osteoclast differentiation in antioxidant-dependent and independent manners, Redox Biol. 48 (2021) 102180.
[12] K. Hu, B.R. Olsen, Osteoblast-derived VEGF regulates osteoblast differentiation and bone formation during bone repair, J. Clin. Investig. 126 (2) (2016) 509–526.
[13] Warren A, Porter RM, Reyes-Castro O, et al. The NAD salvage pathway in mesenchymal cells is indispensable for skel etal development in mice. Nat. Commun.14(1):3616.
[14] P. Pantiya, C. Thonusin, B. Ongnok, et al., Chronic D-galactose administration induces natural aging characteristics, in rat's brain and heart, Toxicology 492 (2023) 153553.
[15] P. Xia, M. Marjan, Z. Liu, et al., Chrysophanol postconditioning attenuated cerebral ischemia-reperfusion injury induced NLRP3-related pyroptosis in a TRAF6-dependent manner, Exp. Neurol. 357 (2022) 114197.
[16] J. Li, M. Tian, T. Hua, et al., Combination of autophagy and NFE2L2/NRF2 activation as a treatment approach for neuropathic pain, Autophagy 17 (12) (2021) 4062–4082.
[17] L. Bai, Y. Liu, X. Zhang, et al., Osteoporosis remission via an anti-inflammaging effect by icariin activated autophagy, Biomaterials 297 (2023) 122125.
[18] X. Li, C. Li, W. Zhang, Y. Wang, P. Qian, H. Huang, Inflammation and aging: signaling pathways and intervention therapies, Signal Transduct. Targeted Ther. 8 (1) (2023) 239.
[19] H. Liu, Q. Xu, H. Wufuer, et al., Rutin is a potent senomorphic agent to target senescent cells and can improve chemotherapeutic efficacy, Aging Cell 23 (1) (2024) e13921.
[20] T. Muto, M. Guillamot, J. Yeung, et al., TRAF6 functions as a tumor suppressor in myeloid malignancies by directly targeting MYC oncogenic activity, Cell Stem Cell 29 (2) (2022) 298–314.e299.
[21] S. Murakami, Y. Kusano, K. Okazaki, T. Akaike, H. Motohashi, NRF2 signalling in cytoprotection and metabolism, Br. J. Pharmacol. (2023), https://doi.org/10.1111/bph.16246.
[22] M. Yamamoto, T.W. Kensler, H. Motohashi, The KEAP1-NRF2 system: a Thiol-based sensor-effector apparatus for maintaining redox homeostasis, Physiol. Rev. 98 (3) (2018) 1169–1203.
[23] C. Xie, M. Ge, J. Jin, et al., Mechanism investigation on Bisphenol S-induced oxidative stress and inflammation in murine RAW264.7 cells: the role of NLRP3 inflammasome, TLR4, Nrf2 and MAPK, J. Hazard Mater. 394 (2020) 122549.
[24] X. Sun, Z. Xie, B. Hu, et al., The Nrf2 activator RTA-408 attenuates osteoclastogenesis by inhibiting STING dependent NF-κb signaling, Redox Biol. 28 (2020) 101309.
[25] L. Wei, W. Chen, L. Huang, et al., Alpinetin ameliorates bone loss in LPS-induced inflammation osteolysis via ROS mediated P38/PI3K signaling pathway, Pharmacol. Res. 184 (2022) 106400.
[26] S.A. Rushworth, L. Zaitseva, M.Y. Murray, N.M. Shah, K.M. Bowles, D.J. MacEwan, The high Nrf2 expression in human acute myeloid leukemia is driven by NF-κB and underlies its chemo-resistance, Blood 120 (26) (2012) 5188–5198.
[27] Liu L, Wu W, Li J, et al. Two sesquiterpene aminoquinones protect against oxidative injury in Ha CaT keratinocytes via activation of AMPKα/ERK-Nrf2/ARE/HO-1 signaling. Biomed. Pharmacother.100:417-425.
[28] Xie X, Hu L, Mi B, et al. SHIP1 activator AQX-1125 regulates osteogenesis and osteoclastogenesis through PI3K/Akt and NF-κb signaling. Front. Cell Dev. Biol.10: 826023.
[29] A.A. Widjaja, W.W. Lim, S. Viswanathan, et al., Inhibition of IL-11 signalling extends mammalian healthspan and lifespan, Nature 632 (8023) (2024) 157–165.
[30] Melough MM, Sun X, Chun OK. The role of AOPP in age-related bone loss and the potential benefits o f Berry Anthocyanins. Nutrients.9(7):789.
[31] M. He, H.H. Chiang, H. Luo, et al., An Acetylation switch of the NLRP3 inflammasome regulates aging-associated chronic inflammation and insulin resistance, Cell Metab. 31 (3) (2020) 580–591.e585.
[32] Y. Li, Q. Zhuang, L. Tao, et al., Urolithin B suppressed osteoclast activation and reduced bone loss of osteoporosis via inhibiting ERK/NF-κB pathway, Cell Prolif. 55 (10) (2022) e13291.
[33] V. Deepak, S.T. Yang, Z. Li, et al., IFT80 negatively regulates osteoclast differentiation via association with Cbl-b to disrupt TRAF6 stabilization and activation, Proc. Natl. Acad. Sci. U. S. A 119 (26) (2022) e2201490119.
[34] D.J. Wu, I.E. Adamopoulos, Loss of WDFY3 ameliorates severity of serum transfer-induced arthritis independently of autophagy, Cell. Immunol. 316 (2017) 61–69.
[35] D.J. Wu, R. Gu, R. Sarin, et al., Autophagy-linked FYVE containing protein WDFY3 interacts with TRAF6 and modulates RANKL-induced osteoclastogenesis, J. Autoimmun. 73 (2016) 73–84.
[36] J.N. Farr, E.J. Atkinson, S.J. Achenbach, et al., Effects of intermittent senolytic therapy on bone metabolism in postmenopausal women: a phase 2 randomized controlled trial, Nat. Med. 30 (9) (2024) 2605–2612.
[37] B. Guo, Z. Zuo, X. Di, et al., Salidroside attenuates HALI via IL-17A-mediated ferroptosis of alveolar epithelial cells by regulating Act1-TRAF6-p38 MAPK pathway, Cell Commun. Signal. : CCS 20 (1) (2022) 183.
[38] L. Feng, R.R. Shang, X.J. Wang, et al., The natural alkaloid (-)-N-hydroxyapiosporamide suppresses colorectal tumor progression as an NF-κB pathway inhibitor by targeting the TAK1-TRAF6 complex, J. Nat. Prod. 86 (6) (2023) 1449–1462.
[39] S. Tao, S.Q. Chen, W.T. Zhou, et al., A novel biocompatible, simvastatin-loaded, bone-targeting lipid nanocarrier for treating osteoporosis more effectively, RSC Adv. 10 (35) (2020) 20445–20459.
[40] Q. Wa, Y. Luo, Y. Tang, et al., Mesoporous bioactive glass-enhanced MSC-derived exosomes promote bone regeneration and immunomodulation in vitro and in vivo, J. Orthopaedic Translat. 49 (2024) 264–282.
[41] K. Marycz, A. Smieszek, K. Marcinkowska, et al., Nanohydroxyapatite (nHAp) doped with iron oxide nanoparticles (IO), miR-21 and miR-124 under magnetic field conditions modulates osteoblast viability, reduces inflammation and inhibits the growth of osteoclast - a novel concept for osteoporosis treatment: Part 1, Int. J. Nanomed. 16 (2021) 3429–3456.